THE JOURNAL OF BIOLOGICAL CHEMISTRY VOL. 290, NO. 8, pp. 4772–4783, February 20, 2015

The Atlastin C-terminal Tail Is an Amphipathic Helix That Perturbs the Bilayer Structure during Endoplasmic Reticulum Homotypic Fusion

Received for publication, August 7, 2014, and in revised form, December 19, 2014 Published, JBC Papers in Press, January 2, 2015, DOI 10.1074/jbc.M114.601823

Joseph E. Faust[‡1], Tanvi Desai[‡1], Avani Verma[‡1], Idil Ulengin[§], Tzu-Lin Sun[¶], Tyler J. Moss[‡], Miguel A. Betancourt-Solis[‡], Huey W. Huang[¶2], Tina Lee[§3], and James A. McNew[‡4]

From the [‡]Department of Biochemistry and Cell Biology, Rice University, Houston Texas 77005, the [§]Department of Biological Sciences, Carnegie Mellon University, Pittsburgh, Pennsylvania 15213, and the [¶]Department of Physics and Astronomy, Rice University, Houston, Texas 77005

Background: Atlastin is large GTPase that catalyzes the homotypic fusion of ER membranes.
Results: *In vitro* and *in vivo* studies reveal that the C-terminal tail of Atlastin affects its function.
Conclusion: The amphipathic C-terminal tail of Atlastin destabilizes lipid bilayers to promote membrane fusion.
Significance: Describing the mechanism of Atlastin-mediated fusion is a critical step in our understanding of ER structure formation.

Fusion of tubular membranes is required to form three-way junctions found in reticular subdomains of the endoplasmic reticulum. The large GTPase Atlastin has recently been shown to drive endoplasmic reticulum membrane fusion and three-way junction formation. The mechanism of Atlastin-mediated membrane fusion is distinct from SNARE-mediated membrane fusion, and many details remain unclear. In particular, the role of the amphipathic C-terminal tail of Atlastin is still unknown. We found that a peptide corresponding to the Atlastin C-terminal tail binds to membranes as a parallel α helix, induces bilayer thinning, and increases acyl chain disorder. The function of the C-terminal tail is conserved in human Atlastin. Mutations in the C-terminal tail decrease fusion activity *in vitro*, but not GTPase activity, and impair Atlastin function *in vivo*. In the context of unstable lipid bilayers, the requirement for the C-terminal tail is abrogated. These data suggest that the C-terminal tail of Atlastin locally destabilizes bilayers to facilitate membrane fusion.

The structure and function of intracellular organelles, particularly those in the secretory pathway, rely heavily on membrane and content exchange. In most cases, this exchange is accomplished by regulated membrane fusion. Cargo transport throughout the secretory pathway depends on specific targeting and fusion of the vesicular intermediates by SNARE proteins and their associated regulatory factors. The mechanism by which SNARE proteins drive membrane fusion is fairly well established (1, 2). However, membrane fusion events within the endomembrane system are still poorly characterized (3).

The morphology and function of the endoplasmic reticulum is inextricably linked to architectural shape changes. The interconnected network of ER[5] tubules and sheets makes physical contact with virtually every cytoplasmic organelle (3). The dynamic nature of ER tubules allows for rapid shape changes that likely correspond to differences in functional interaction (4, 5). One of the major players involved in ER shape is the membrane fusion protein Atlastin (6). We and others have shown that the GTPase Atlastin drives the fusion of ER tubules and that this fusion reaction is vitally important for the overall function of this organelle (6, 7) Atlastin interacts with a variety of other proteins resident within the ER, like the ER shape-forming proteins reticulon, receptor expression-enhancing protein (REEP), and DP1 (7); spastin (8, 9); and luna park (10).

The mechanism by which Atlastin fuses ER membranes is beginning to be elucidated. We know that membrane fusion requires GTPase activity (6, 7), oligomerization (11), and structural elements within the extreme carboxyl terminus of the protein (11, 12). In this work, we examine the requirements and characteristics of the C-terminal juxtamembrane amphipathic α helix. We found that a peptide corresponding to 23 amino acids immediately after the second transmembrane domain forms a helix in the presence of membranes and directly interacts with membrane surfaces. We also show that membrane interaction alters the physical properties of the bilayer, such as membrane thinning and disorganization of fatty acid acyl chains. Targeted point mutations within the hydrophobic face of the amphipathic helix resulted in reduced membrane fusion *in vitro*, consistent with a role for amphipathic destabilization during the membrane fusion cycle. Additionally we found that *Drosophila* Atlastin functions in mammalian cells, where it also

[1] These authors contributed equally to this work.
[2] Supported by National Institutes of Health Grant GM55203 and Robert A. Welch Foundation Grant C-0991.
[3] Supported by National Institutes of Health Grant GM107285.
[4] Supported by National Institutes of Health Grant GM101377, by The Virginia and L. E. Simmons Family Foundation, and by The Hamill Foundation. To whom correspondence should be addressed: Dept. of Biochemistry and Cell Biology, Rice University, 6100 Main St. Rice University, MS601, Houston, TX 77005. Tel.: 713-348-3133; E-mail: mcnew@rice.edu.

[5] The abbreviations used are: ER, endoplasmic reticulum; POPC, 1-palmitoyl-2-oleoyl-*sn*-glycero-3-phosphocholine; DOPS, 1,2-dioleoyl-*sn*-glycero-3-phospho-L-serine; DOPE, dioleoylphosphatidylethanolamine; PC, phosphatidylcholine; PS, phosphatidylserine; NBD, nitrobenzoxadiazole; DPPE, [3H]1-palmitoyl 2-palmitoylphosphatidylethanolamine; PE, phosphatidylethanolamine.

requires its C-terminal tail. Somewhat surprisingly, we found that mutations within the C-terminal helix were much more tolerated *in vivo* than *in vitro*. This result is likely because of alterations in the lipid composition of native membranes *versus* synthetic membranes used in *in vitro* fusion. We tested this directly by altering the lipid composition of synthetic proteoliposomes and found that phosphatidylethanolamine, which promotes non-bilayer-forming structures, can help alleviate the requirement for the C-terminal tail. In total, these results establish that the Atlastin C-terminal tail is a membrane-perturbing α helix that participates in membrane fusion by destabilizing the bilayer structure and promoting the mechanics of lipid mixing.

EXPERIMENTAL PROCEDURES

Molecular Biology

A bacterial expression vector containing GST fused to *Drosophila* Atlastin (dAtl) with a C-terminal octahistidine tag (pJM681) has been described previously (6). The construct pJM706 (GST-dAtl$^{1-471}$-His$_8$) has been described previously (11). The construction of other clones was carried out as detailed below.

pJM882 (GST-dAtl(L482K)-His$_8$)—The point mutation L482K was generated by overlap PCR using the primers DAtl L482K forward (CGACTTTGGCGGCAAGAAGGATGACTTTGCAAC) and dAtl L482K reverse (GTTGCAAAGTCATCCTTCTTGCCGCCAAAGTCG). The point mutation PCR product was further amplified by PCR using the primers BamHI-Dm_Atl (CCGGATCCATGGGCGGATCGGC) and Dm_Atl-XhoI (without stop) (ATCTCGAGTGACCGCTTCACC). The PCR product was then digested with BamHI and XhoI and ligated into pJM681 cut with the same enzymes.

pJM863 (GST-dAtl(F478K)-His$_8$)—The point mutation F478K was generated by overlap PCR using the primers dAtl F478K forward (GGAGAGCTCAGCGACAAAGGCGGCAAGTTGGATG) and dAtl F478K reverse (CATCCAACTTGCCGCCTTTGTCGCTGAGCTCTCC). The point mutation PCR product was further amplified by PCR using the primers BamHI-Dm_Atl (CCGGATCCATGGGCGGATCGGC) and Dm_Atl-XhoI (without stop) (ATCTCGAGTGACCGCTTCACC). The PCR product was then digested with BamHI and XhoI and ligated into pJM681 cut with the same enzymes.

pJM928 (GST-dAtl(F478K,L482K)-His$_8$)—The point mutations F478K and L482K were generated by overlap PCR using the primers dAtl F478K L482K forward (CTCAGCGACAAAGGCGGCAAGAAGGATGACTT) and dAtl F478K L482K reverse (AAGTCATCCTTCTTGCCGCCTTTGTCGCTGAG). The point mutation PCR product was further amplified by PCR using the primers BamHI-Dm_Atl (CCGGATCCATGGGCGGATCGGC) and Dm_Atl-XhoI (without stop) (ATCTCGAGTGACCGCTTCACC). The PCR product was then digested with BamHI and XhoI and ligated into pJM681 cut with the same enzymes.

pJM866 (GST-dAtl(Human Atl-1 C-terminal tail)-His$_8$)—The Hs-Atl1 C-terminal tail was generated by PCR using the primers BspEI-Hsatl1-c-tail (ATTCCGGAGAATACCGAGAGCTGG) and Hs_Atl_XhoI (TTCTCGAGCATTTTTTTCTTTTC). The PCR product was digested with BspEI and XhoI and ligated into pJM681 cut with the same enzymes.

pJM868 (GST-dAtl(Human Atl-3 C-terminal tail)-His$_8$)—The Hs-Atl3 C-terminal tail was generated by PCR using the primers BspEI-Hsatl3-c-tail (ATTCCGGACAATATCGTGAGCTGGGC) and Hs_Atl_XhoI (TTCTCGAGCATTTTTTTCTTTTC). The PCR product was digested with BspEI and XhoI and ligated into pJM681 cut with the same enzymes.

pJM1082 (GST-dAtl(L482K,A486D,L489D,F493D)-His$_8$)—A gene fragment corresponding to residues 461–541 of dAtl, containing the L482K, A486D, L489D, and F493D point mutations, was synthesized by Integrated DNA Technology, cut with SacI and XhoI, and ligated into pJM681 cut with the same enzymes.

pJM1084 (GST-dAtl(G480K)-His$_8$)—A gene fragment corresponding to residues 461–541 of dAtl, containing the G480K point mutation, was synthesized by Integrated DNA Technology, cut with SacI and XhoI, and ligated into pJM681 cut with the same enzymes.

pJM850 (Venus-dAtl)—Venus was PCR-amplified from Venus-GRX2 in pET28a (a gift from Joff Silberg (13)) using the oligos KpnI Venus A (CGGGTACCATGGTGAGCAAG) and Venus-BamHI 3′ (TAGGATCCGGGCCCAGCCTTGTA), cut with KpnI and BamHI, and ligated into pcDNA3.1 cut with the same enzymes. dAtl was PCR-amplified from pJM681 using the oligos BamHI-Dm_Atl (CCGGATCCATGGGCGGATCGGC) and Dm_Atl-XhoI (ATCTCGAGTCATGACCGCTTCACC), cut with BamHI and XhoI, and ligated into Venus in pcDNA3.1 cut with the same enzymes.

pJM1002 (Venus-dAtl(1–471)-KKXX)—dAtl(1–471)-KK*XX* was PCR-amplified from pJM706 using the oligos BamHI-Dm_Atl (CCGGATCCATGGGCGGATCGGC) and Dm_atl(1–471)-GKVKRS-Stop-XhoI (CCCTCGAGTCATGACCGCTTCACCTTGCCATATCTAATGTAGGCCCAC), cut with BamHI and XhoI, and ligated into pJM850 cut with the same enzymes.

pJM1004 (Venus-dAtl(L482K))—dAtl(L482K) was PCR-amplified from pJM882 using the oligos BamHI-Dm_Atl (CCGGATCCATGGGCGGATCGGC) and Dm_Atl-XhoI (ATCTCGAGTCATGACCGCTTCACC), cut with BamHI and XhoI, and ligated into pJM850 cut with the same enzymes.

pJM1005 (Venus-datl(K51A))—dAtl(K51A) was PCR-amplified from pJM694 (GST-Dm-Atlastin (K51A) His$_8$) using the oligos BamHI-Dm_Atl (CCGGATCCATGGGCGGATCGGC) and Dm_Atl-XhoI (ATCTCGAGTCATGACCGCTTCACC), cut with BamHI and XhoI, and ligated into pJM850 cut with the same enzymes.

The following mutants were generated using QuikChange site-directed mutagenesis PCR (Qiagen) and fully verified by sequencing.

Venus-dAtl (A486D)—The point mutation A486D was generated using the QuikChange primers dAtl A486D forward (GGCAAGTTGGATGACTTTGATACGCTATTGTGGGAG) and dAtl A486D reverse (CTC CCA AATAGCGTATCAAAGTCATCCAACTTGCC) with pJM850 as a template.

Venus-dAtl (L482K;A486D;L489D)—The triple point mutation was generated using the QuikChange primers dAtl_L482K_A486D_L489D forward (GGCAAGAAGGATGACTTTGATACGCTAGATTGGGAGAAATTCATGCGACCC)

and dAtl_L482K_A486D_L489D reverse (GGGTCGCATGAATTTCTCCCAATCTAGCGTATCAAAGTCATCCTTCTTGCC) with pJM850 as a template.

Venus-dAtl (L482K;A486D;L489D;F493D)—The quadruple mutant was generated using the QuikChange primers dAtl_L482K_A486D_L489D_F493D forward (CGCTAGATTGGGAGAAAGACATGCGACCCATCTATCACGGCTGC) and DAtl_L482K_A486D_L489D_F493D reverse (GCAGCCGTGATAGATGGGTCGCATGTCTTTCTCCCAATCTAGCG) using Venus-dAtl (L482K;A486D;L489D) DNA as the template.

Peptide Production

Two peptides, RYSGELSDFGGKLDDFATLLWEK (C23) and RYSGELSDKGGKKDDFATLLWEK (C23-KK), corresponding to the C-terminal tail of *Drosophila* Atlastin, were purchased from GenScript. The peptides contained an N-terminal acetylation and a C-terminal amidation.

Large Unilamellar Vesicle Preparation, Circular Dichroism, and X-ray Diffraction

1-palmitoyl-2-oleoyl-*sn*-glycero-3-phosphocholine (POPC) and 1,2-dioleoyl-*sn*-glycero-3-phospho-L-serine (DOPS) were purchased from Avanti Polar Lipids (Alabaster, AL). POPC and DOPS were mixed in a 85:15 molar ratio. Dried lipids were resuspended in Tris buffer solution (10 mM (pH 7)) to 1 mg/ml. This stock was fully mixed and exposed to more than five freeze-thaw cycles. A mini-extruder from Avanti Polar Lipids and Whatman Nuclepore Track-Etch 0.2-μm filters from GE Healthcare were used to produce liposomes. CD, oriented CD, and x-ray diffraction experiments were performed as described previously (14, 15).

Proteoliposome Production

Proteins purified in 0.1% Anapoe X-100 (Anatrace) were reconstituted into preformed 100-nm liposomes as described previously (6). Liposomes were made by extrusion. Lipid mixtures used were as follows: unlabeled (POPC) and labeled lipid mixtures (POPC:Rhodamine-DPPE:NBD-DPPE, 97:1.5:1.5 mole ratio), unlabeled lipid mixtures (POPC:DOPS, 85:15 molar ratio) and labeled lipid mixtures (POPC:DOPS:Rhodamine-DPPE:NBD-DPPE, 82:15:1.5:1.5 molar ratio), unlabeled lipid mixtures (POPC:DOPS:DOPE, 75:15:10 molar ratio) and labeled lipid mixtures (POPC:DOPS:DOPE:Rhodamine-DPPE:NBD-DPPE, 75:15:7:1.5:1.5 molar ratio), and unlabeled lipid mixtures (POPC:DOPS:DOPE, 65:15:20 molar ratio) and labeled lipid mixtures (POPC:DOPS:DOPE:Rhodamine-DPPE:NBD-DPPE, 65:15:17:1.5:1.5 molar ratio).

Lipid mixtures with trace amounts of 3*H*-1-palmitoyl 2-palmitoylphosphatidylethanolamine (DPPE) in chloroform were dried under a stream of nitrogen gas, followed by further drying in a vacuum for 30 min. The lipid films were resuspended in A100 + 10% glycerol, 2 mM 2-mercaptoethanol, and 1 mM EDTA to a final total lipid concentration of ~10 mM. Large unilamellar vesicles were formed by ten freeze-thaw cycles in liquid N_2 and room temperature water. Uniform-sized large unilamellar vesicles were formed by extrusion through polycarbonate filters with 100-nm pore size (Avanti Polar Lipids).

Protein Expression and Purification

GST-tagged proteins were purified starting by transforming *Escherichia coli* BL21(DE3) (Stratagene) cells with the respective expression plasmid. Overnight colonies were picked to start pre-precultures in 5 ml LB + ampicillin. The pre-precultures were used to start 50 ml precultures that were grown overnight at 25 °C. The cells from the 50-ml precultures were pelleted at 3000 rpm (~2000 × *g*) for 15 min using an Allegra tabletop centrifuge at room temperature. The cell pellet was used to seed 2- to 4-liter cultures with a starting density of about 0.1–0.2 OD_{600}. The cultures were grown at 25 °C up to a desirable density (OD = 0.4 to 0.6), at which time the culture was moved to a 16 °C incubator. Ten minutes after growth at 16 °C, protein expression was induced with 0.2 mM isopropyl 1-thio-β-d-galactopyranoside, and the cultures were grown overnight (~16 h) at 16 °C. The cells were harvested, washed with A200 (25 mM HEPES (pH 7.4) and 200 mM KCl) and lysed in breaking buffer (A200 + 10% glycerol, 2 mM 2-mercaptoethanol (βME), 4% Triton X-100, and 1× complete protease inhibitor mixture (Roche)) by passage through an Emulsiflex C-3 high-pressure homogenizer (Avestin) twice at 15,000–20,000 p.s.i. Cell extracts were cleared by centrifugation at 125,000 × *g* (~186,000 × *g*) for 30 min using a Type 45-Ti rotor in an Optima LE-80K ultracentrifuge (Beckman) cooled to 4 °C. Cleared extracts were incubated with nickel Fast Flow beads for 30 min at 4 °C. The nickel bead-bound protein was washed with 10 ml of A400 (25 mM HEPES (pH 7.4) and 400 mM KCl) plus 10% glycerol, 2 mM βME, and 1% Triton X-100. The cells were then washed with 10 ml of A100 (25 mM HEPES (pH 7.4) and 100 mM KCl) plus 10% glycerol, 2 mM βME, and 1% Triton X-100 and then washed again with 10 ml of A100 plus 10% glycerol, 2 mM βME, 1% Triton X-100, and 0.1 M imidazole. The nickel-bound protein was then eluted with A100 plus 10% glycerol, 2 mM βME, 1% Triton X-100, and 0.5 M imidazole twice. The elutions were combined and incubated with 90 mg of swollen GSH-agarose beads (Sigma) for 1 h at 25 °C. The GSH bead-bound protein was washed with A100 plus 10% glycerol, 2 mM βME, 1% Triton X-100, and 1 mM EDTA. The protein was washed five more times with 10 ml of A100 plus 10% glycerol, 2 mM βME, 0.1% Anapoe X-100, and 1 mM EDTA. The protein was eluted from GSH-agarose with A100 plus 10% glycerol, 2 mM βME, 0.1% Anapoe X-100, 1 mM EDTA, and 10 mM GSH.

Proteins were analyzed by SDS-PAGE, and concentrations were determined by Amido Black protein assay (16). Frozen aliquots were stored at −80 °C.

Reconstitution

Atlastin and Atlastin mutants were reconstituted into both labeled and unlabeled 100-nm liposomes by a detergent-assisted insertion method (17, 18) as follows. dAtl in 0.1% Anapoe X-100 was mixed with preformed liposomes at a 1:400 protein:lipid molar ratio and an effective detergent:lipid ratio of ~0.8. The effective detergent:lipid ratio (R_{eff}) was determined by the equation $R_{eff} = D_{total} - D_{water} / [lipid]$, where D_{total} is the total detergent concentration and D_{water} is the monomeric detergent concentration (0.18 mM) in the presence of lipid. Protein and lipid were allowed to mix for 1 h at 4 °C. The detergent was

removed by Bio-Beads SM-2 adsorbent (Bio-Rad) at 70 mg of Triton X-100/1 g of beads. Insoluble protein aggregates were pelleted by centrifugation of the samples in an Eppendorf microcentrifuge (10 min at 16,000 × *g* (max)). Final lipid and protein concentrations were determined by liquid scintillation counting and Amido Black protein assay (16), respectively. Protein:lipid ratios ranged from ~1:400–1:600, and protein concentrations ranged from ~1.5–2.5 μM. Reconstitution efficiencies were not dependent on protein or lipid composition.

In Vitro Fusion Assays

Fusion assays were performed on the basis of a method described previously (6), with the following modifications. Labeled and unlabeled populations of Atlastin or mutant Atlastin proteoliposomes (0.15 mM lipid each) were mixed in the presence of 0.5 mM GTP or buffer only and brought to a total volume of 45 μl with A100 buffer in wells of 96-well FluoroNunc PolySorp plates (Nunc). The reactants in the plate were incubated at 37 °C in a fluorescent plate reader (Infinite M200, Tecan) for 5 min. To each well, 5 μl of 50 mM $MgCl_2$ was added, and nitrobenzoxadiazole (NBD) fluorescence was measured (excitation 460 nm, emission 538 nm) at 1-min intervals for 60 min with a 1-s shaking after every reading. To determine the absolute NBD fluorescence, 10 μl of 2.5% (w/v) *n*-dodecylmaltoside was added at 60 min. Data were normalized to total fluorescence after detergent solubilization.

GTPase Measurements

GTPase activity was measured as described previously (6) by measuring the release of inorganic phosphate from GTP, as suggested by the EnzChek phosphate assay kit (Molecular Probes). Recombinant Atlastin and Atlastin mutants were mixed in a 100-μl reaction volume with 1 unit/ml purine nucleoside phosphorylase, 200 μM 2-amino-6-mercapto-7-methylpurine riboside, and GTP in a transparent 96-well plate. The plates were warmed to 37 °C in a microplate reader (Infinite M200, Tecan), and 5 mM Mg^{2+} was added to start the reaction. In the presence of inorganic phosphate, purine nucleoside phosphorylase catalyzes the conversion of 2-amino-6-mercapto-7-methylpurine riboside to ribose 1-phosphate and 2-amino-6-mercapto-7-methylpurine, resulting in a spectrophotometric shift in absorbance from 330 to 360 nm. The absorbance increase at 360 nm was measured in real time approximately every 20 s over 20 min. Absorbance was normalized to phosphate standards, and initial rates were calculated.

Measurement of Tryptophan Fluorescence

The dAtl C-terminal tail peptide (45 μM) and liposomes (9.5 mM) were mixed in a Greiner half area plate (black). The total volume was adjusted to 50 μl with A100 buffer. Blank samples contained liposomes but no peptide. All samples were excited at 278 nm in a spectrofluorometer (Infinite M200, Tecan), and emission was measured between 300–500 nm.

Cell Culture and Atlastin Knockdown

HeLa cell culture, knockdown, and imaging were performed as described previously (19).

RESULTS

The Atlastin C-terminal Tail Is an Amphipathic Helix and Interacts with Membranes—We have shown recently that the Atlastin C-terminal 23 amino acids are required for membrane fusion *in vitro* and *in vivo* (11). Bioinformatic analysis suggests that this segment of Atlastin is an amphipathic helix (Ref. 11 and Fig. 1*A*). We next wanted to probe this requirement more deeply by examining the interaction of a peptide corresponding to this region with membranes. First, we used a native tryptophan residue (amino acid 490 of *Drosophila* Atlastin) in the C-terminal peptide (C23) to examine the propensity of the peptide to associate with membranes. Liposomes containing pure phosphatidylcholine or a mixture of 85 mol% phosphatidylcholine and 15 mol% phosphatidylserine were incubated with or without peptide, and intrinsic tryptophan fluorescence was determined. Fig. 1*B* shows that the C-terminal peptide is membrane-active and binds to both membrane compositions, with a slight preference for membranes with no charge (Fig. 1*B*, *green trace*). These results are in agreement with a recent study that determined that a similar peptide from *Drosophila* Atlastin bound to membranes and could supply the required function in *trans* (20).

The Atlastin C-terminal Amphipathic Helix Perturbs Lipid Bilayers—CD (Fig. 1*D*) suggests that C23 is largely unstructured in solution (*blue circles*), even in the presence of liposomes (*red circles*). However, the α-helical secondary structure parallel to the surface of the bilayer was observed by oriented CD (Fig. 1*E*) when the peptide was located between membranes of a multilayered structure.

We hypothesize that the primary function of the amphipathic C-terminal tail is to destabilize membrane structure during Atlastin-mediated membrane fusion. To test the effects of the C-terminal peptide on membrane structure, we employed x-ray diffraction to measure lipid organization in the presence of the peptide (21). Fig. 1, *F* and *G*, shows characteristic changes to membrane structures that are consistent with bilayer perturbation. The presence of the peptide results in an overall bilayer thinning, indicated by a reduced phosphate-to-phosphate distance with an increase in peptide concentration (Fig. 1, *F* and *G*) by about 10% (~38–34 Å). Additionally, the presence of the peptide resulted in a broadening of the trough of minimal x-ray intensity within the hydrophobic phase of the bilayer, indicative of acyl chain disorder (Fig. 1*F*). Overall, the Atlastin C-terminal tail peptide binds parallel to the surface of membranes as an α helix to induce bilayer thinning and acyl chain disorder, two properties important for the lipid rearrangements that occur during membrane fusion (1–3, 22–24).

The Amphipathic Character of the C-terminal Juxtamembrane Tail of Atlastin Is Conserved Across Species—We tested the functional conservation of the membrane-perturbing properties of this sequence by constructing chimeric *Drosophila* Atlastins that contain the entire C-terminal tail of human Atlastin-1 or human Atlastin-3 (Fig. 2). The loss of the tail eliminates fusion under most conditions (11, 20), but the presence of the human tails restores *in vitro* fusion to ~50% of the wild-type protein. This level of recovery is comparable with replacing the entire 60-amino acid tail with the juxtamembrane-conserved 23 amino acids (11). The ability of these *Dros-*

ophila-human chimeras to support *in vitro* fusion confirms that the membrane-destabilizing characteristics of the amphipathic helix are also conserved across species.

Alteration of the Hydrophobic Face of the Amphipathic Helix Reduces Membrane Fusion—The characteristic repeat structure of an amphipathic helix can be disrupted by replacing hydrophobic side chains that normally interact with the membrane with charged side chains. We generated several mutant Atlastins that alter the hydrophobic face, three of which are reported below. These include F478K, L482K, and the double mutant (F478K/L482K). These mutants were produced, reconstituted into proteoliposomes, and fused. Introduction of a sin-

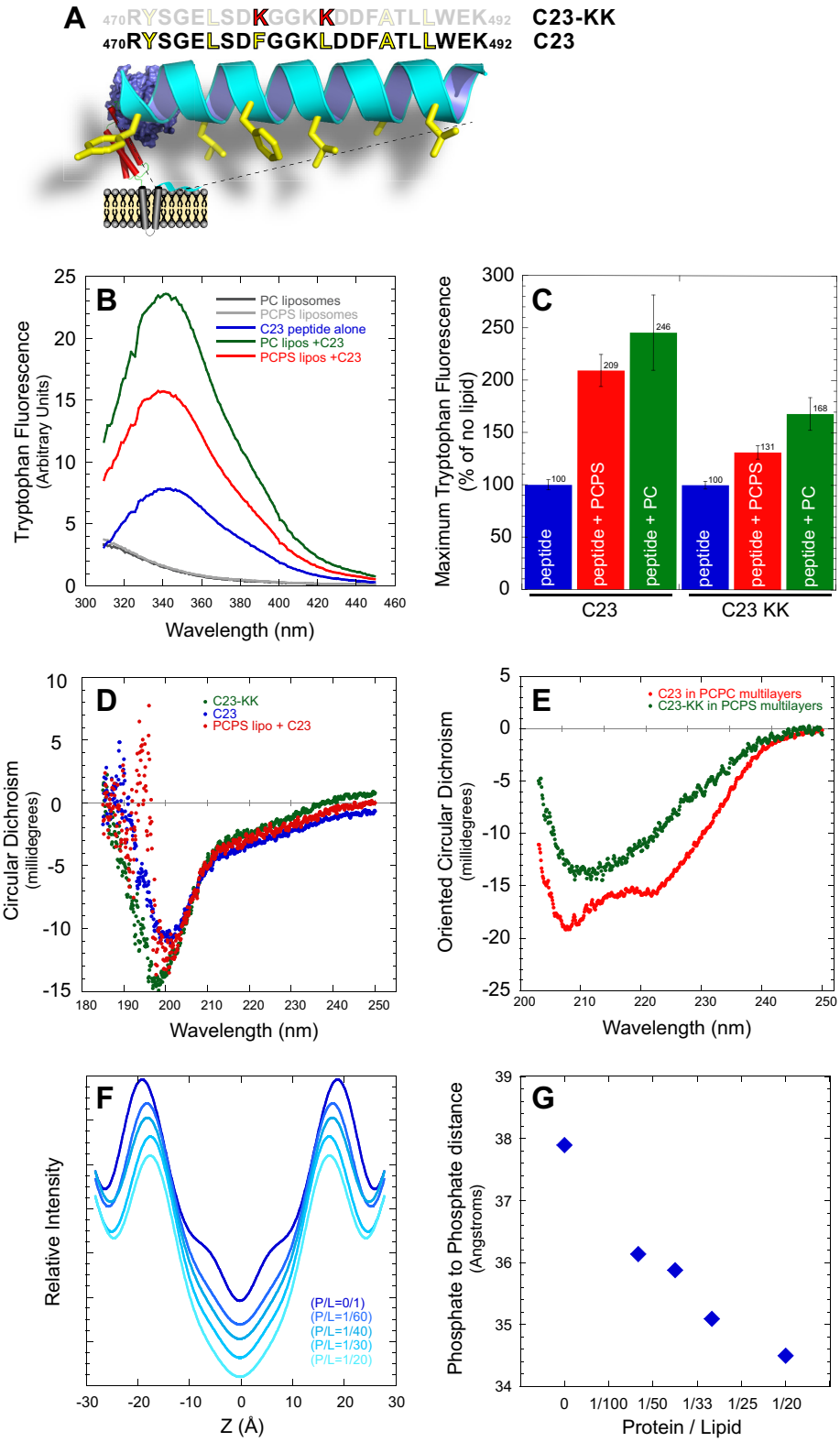

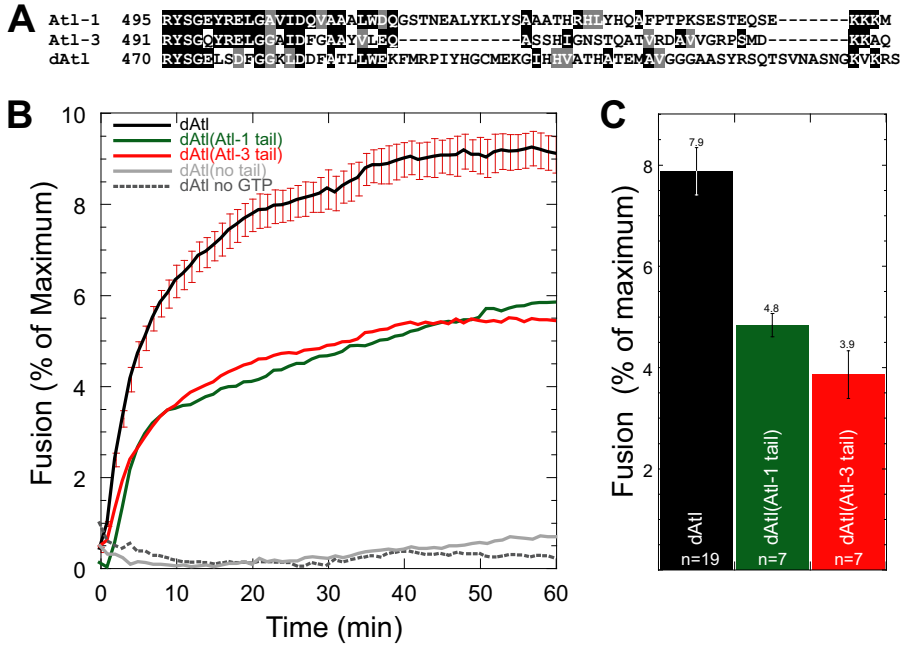

FIGURE 2. **The Amphipathic character of the C-terminal tail is conserved across species.** *A*, alignment of the C-terminal cytoplasmic tail of human Atlastins and *Drosophila* Atlastin. *Highlighted portions* show highly conserved residues following the transmembrane domain. *B*, kinetic fusion graph of unlabeled dAtl acceptor proteoliposomes fused with equimolar amounts of fluorescently labeled dAtl donor proteoliposomes. NBD fluorescence was measured at 1-min intervals, and detergent was added at 60 min to determine maximum fluorescence. In all cases, the same dAtl mutant is reconstituted into both liposome populations. All fusion experiments are $n = 6$. *Black*, WT GST-dAtl-His_8; *green*, GST-dAtl(Atl1-tail)-His_8; *red*, GST-dAtl(Atl-3-tail)-His_8; *solid gray*, GST-dAtl(1–471)-His_8; *dashed gray*, control reaction in the absence of GTP. *C*, the extent of fusion at 60 min is represented in a histogram as the percentage of fusion. *Error bars* show mean ± S.E.

gle charge (F478K) close to the membrane interface reduced homotypic fusion by about 35% (Figs. 3, *A* and *C*, *green trace* and *histogram*, and 6), whereas a single charge one turn further down the helix face (L482K) decreased fusion by ~80% (Figs. 3, *A* and *C*, *red trace* and *histogram*, and 6). The double mutant (F478K/L482K), was marginally more effective than either single mutant (~85% reduction; Figs. 3, *A* and *C*, *blue trace* and *histogram*, and 6). A mutation in the C-terminal tail, but not in the hydrophobic face, G480K, did not reduce the fusion activity of Atlastin (Fig. 6).

Mutations in the hydrophobic face also impair the ability of the C-terminal tail to bind membranes. A peptide with the F478K and L482K mutations (C23-KK) shows reduced binding to liposomes (Fig. 1*C*). The C23-KK peptide, like the wild-type C23 peptide, is unstructured in solution (Fig. 1*D*). Unlike C23, C23-KK remains unstructured even when located between lipid bilayers. (Fig. 1*E*).

Given that we conduct fusion reactions with equal amounts of protein and lipid in both the labeled and unlabeled liposome populations, we can also determine the effects of mutations on heterotypic membrane fusion. In these reactions, the mutant Atlastin can be reconstituted in either the fluorescently labeled liposome population or the unlabeled bulk lipid liposome population. The location of the mutation relative to the fluorescent labeled lipid used to determine lipid mixing will influence the apparent effects on fusion. The schematic in Fig. 3*E* illustrates these effects. When we measured heterotypic fusion with the L482K charge mutant, we found an intermediate level of fusion (Fig. 3*B*, *red traces with circles*) compared with homotypic fusion (Fig. 3*B*, *red trace*, *no symbols*). The slight improvement in apparent fusion when the L482K mutation is located in the fluorescently labeled liposome population (Fig. 3*B*, *red trace*, *filled red circles*) can be explained by the population nature of the fusion reaction (Fig. 3*E*).

Drosophila Atlastin Functions in Mammalian Cells—Next we tested the effects of mutations or deletions of the Atlastin tail *in vivo*. Previous studies have examined *Drosophila* expression in mammalian cells (6, 11, 25), primarily for the

FIGURE 1. **The Atlastin C-terminal tail is an amphipathic helix that perturbs the bilayer structure.** *A*, the Atlastin C terminus forms an amphipathic helix. A structural schematic of Atlastin illustrating the C-terminal amphipathic α helix shown in a *cyan ribbon diagram* with the membrane facing hydrophobic side chains, shown as *yellow sticks*. The amino acid sequence of the C23 peptide, composed of residues 470–492, is shown above the schematic helix. The amino acid sequence of the C23-KK peptide, containing the F478K and L482K mutations, is shown above the C23 sequence. *B*, the C23 peptide binds to membranes. Intrinsic tryptophan fluorescence is shown at various wavelengths in the presence or absence of liposomes (*lipos*). The C23 peptide alone (*blue trace*) indicates the intrinsic tryptophan fluorescence of the peptide. A significantly increased tryptophan fluorescence is seen in the presence of liposomes (pure phosphatidylcholine liposomes, *green trace*; PC:PS liposomes, *red trace*). *C*, C23-KK shows reduced binding to liposomes. Tryptophan fluorescence in the presence of liposomes is shown as a percentage of the no lipid signal. *D*, CD spectra of C23 with and without PCPS liposomes and C23-KK are shown in *red*, *blue*, and *green dots*, respectively. The spectra imply that C23 and C23-KK were unstructured in solution or in the presence of liposomes. *E*, raw oriented CD spectra of C23 or C23-KK mixed into multilamellar PCPS bilayers in peptide:lipid ratios of 1:40. The oriented CD curve indicates that C23 formed an α-helical structure parallel to the bilayer surface. C23-KK remained unstructured even in presence of bilayers. *F*, peptide interaction perturbs the bilayer structure. Electron density profiles of the bilayers determined by x-ray diffraction at various peptide:lipid ratios (*P/L*) are shown. *Z* is the distance from the bilayer center. *G*, peptide interaction thins the membrane. The phosphate peak-to-phosphate peak distance was measured for a series of peptide:lipid ratios. Each point is the average phosphate peak-to-phosphate peak distance of two independently prepared samples.

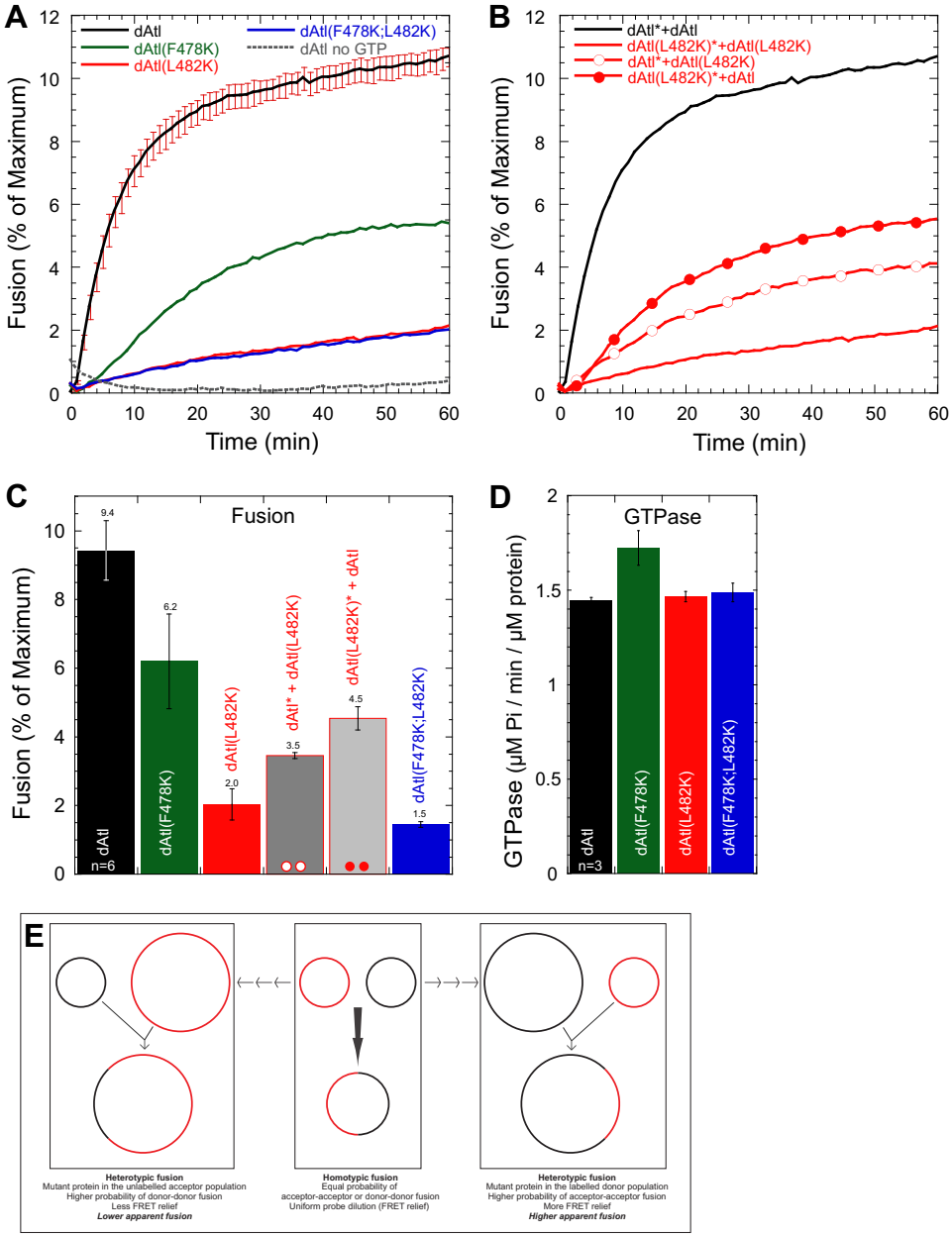

FIGURE 3. **Decreasing the hydrophobicity of the amphipathic tail reduces membrane fusion *in vitro*.** *A*, kinetic fusion graph of unlabeled dAtl acceptor proteoliposomes fused with equimolar amounts of fluorescently labeled dAtl donor proteoliposomes. NBD fluorescence was measured at 1-min intervals, and detergent was added at 60 min to determine maximum fluorescence. In all cases, the same dAtl mutant is reconstituted into both liposome populations. All fusion experiments are $n = 6$. *Black*, WT GST-dAtl-His_8; *green*, GST-dAtl(F478K)-His_8; *red*, GST-dAtl(L482K)-His_8; *blue*, GST-dAtl(F478K; L482K)-His_8; *gray*, control reaction in the absence of GTP. *B*, kinetic fusion graph of heterotypic fusion dAtl proteoliposomes fused with equimolar amounts of GST-dAtl(L482K)-His_8 proteoliposomes. The *asterisk* represents labeled liposomes. *Black*, dAtl*-dAtl; *red*, dAtl(L482K)*-dAtl(L482K); *red*, *open circles*, dAtl*-dAtl (L482K); *red*, *filled circles*, dAtl(L482K)*-dAtl. *C*, the average extent of fusion at 60 min is represented for wild-type and mutant atlastins. All experiments are $n = 6$. *D*, GTPase activity is represented as a histogram for all mutants. All experiments are $n = 3$. *E*, homotypic and heterotypic fusion. Unlabeled acceptor liposomes and shown in *black*. Labeled donor liposomes are shown in *red*. Lower apparent fusion is observed when mutant Atlastin is present only in unlabeled liposomes. Higher apparent fusion is observed when mutant Atlastin is present only in labeled liposomes. Error bars shown mean ± S.E. The numbers in the histograms equal the numbers of replicates.

inability of mutant Atlastins to produce an overexpression phenotype. However, the functionality of *Drosophila* Atlastin in mammalian cells has not been demonstrated. HeLa cells primarily express human Atlastin-2 and Atlastin-3 with little or no Atlastin-1 (19). Knockdown of Atl-2 and Atl-3 by siRNA has proven to be a useful platform to examine Atlastin function by reintroduction of wild-type or mutant proteins (19). Loss of Atl-2 and Atl-3 in HeLa cells results in abnormal ER morphology, manifested as elongated ER tubes with reduced three-way junctions (Ref. 19 and Fig. 4*A*). When wild-type, full-length *Drosophila* Atlastin is reintroduced, normal ER morphology is restored (Fig. 4*B*). The rescued ER morphology is due to *Drosophila* Atlastin function because it is responsive to a dominant GTP binding mutation (K51A) that does not remedy the aberrant ER morphology (Fig. 4*C*). *Drosophila* Atlastin function in HeLa cells also requires the C-terminal amphipathic tail. An Atlastin mutant truncated at residue 471 that removes the C terminus but maintains an

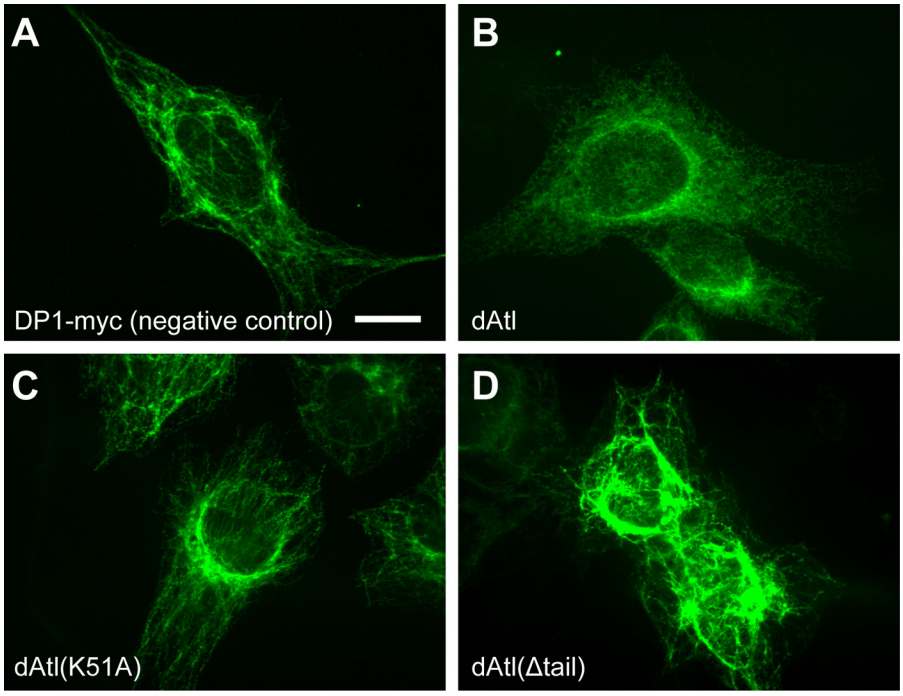

FIGURE 4. ***Drosophila* Atlastin can functionally replace human Atlastin in HeLa cells.** Shown is a knockdown replacement assay. 48 h after transfection with a negative control construct (Myc-tagged DP1, *A*) or the indicated Venus-dAtl constructs, cells were transfected with siRNAs targeting ATL2 and ATL3. 72 h after knockdown, cells were fixed and stained using an antibody against Myc (*A*) or Venus fluorescence (*B–D*) and viewed by confocal microscopy. *A*, HeLa cells transfected with DP1-myc and siRNA targeting Atl-2 and Atl-3 show elongated ER tubules and reduced three-way junctions. *B*, expression of wild-type *Drosophila* atlastin tagged N-terminally with Venus in these cells restores ER morphology. *C*, a GTP binding mutant (Venus-dAtl(K51A)) does not rescue the abnormal ER morphology of siRNA-treated cells. *D*, a mutant lacking the C-terminal amphipathic tail (Venus-dAtl(Δtail)) but maintaining an ER retention signal also fails to rescue the abnormal ER morphology. *Scale bar* = 10 μm.

ER retention signal also fails to recover the ER morphology phenotype (Fig. 4*D*).

Next we determined the effect of C-terminal tail mutations of the amphipathic α helix *in vivo*. Surprisingly, single charge mutations in the C-terminal tail were largely without effect *in vivo* (Figs. 5, *A* and *B*, and 6). We expanded the mutant collection to include multiple mutations down the length of the hydrophobic face. Loss of function required four charge replacements before *in vivo* recovery was lost (Figs. 5*D* and 6). Fig. 6 compares the functional effects of point mutations within the hydrophobic face of the amphipathic helix both *in vitro* and *in vivo*.

Lipid Composition Strongly Affects Requirements for the C-terminal Amphipathic Helix—Taken together, these data confirm that the C-terminal tail is required *in vivo* but that its functionality is much less susceptible to small changes in the physical characteristics of the amphipathic helix. One possible explanation is that even a low level of fusion activity is sufficient to restore the ER network *in vivo*. An alternative, more likely explanation is the substantial difference in lipid composition between the *in vitro* experiments and the *in vivo* result. To test the latter hypothesis directly, we re-examined *in vitro* fusion with an altered lipid composition. We suggest that the fundamental role of the C-terminal helical region is to provide membrane destabilization during the fusion mechanism. This role is supported by effects of the peptide containing this region on lipid bilayer structure. However, alterations in lipid composition can also influence the propensity of a bilayer to undergo the necessary lipid transitions during fusion. If the role of the C-terminal helix is to directly interact with the membrane to destabilize it, then perhaps an inherently more unstable lipid mixture will alleviate the need for this activity.

We produced proteoliposomes that contained increasing concentrations of the non-bilayer-forming lipid phosphatidylethanolamine (PE). The physical properties of PE and its relatively large amount of spontaneous negative curvature allow for membrane structural changes that are required during fusion (26). For this reason, membranes that contain PE are inherently more unstable and easier to fuse. Fig. 7 shows the outcome of *in vitro* membrane fusion reactions with mixtures of wild-type protein and the terminally truncated Atlastin that lacks the amphipathic tail. When wild-type Atlastin is present in both liposome populations, the inclusion of PE at 10 mol% (Fig. 7, *green bar*) or 20 mol% (Fig. 7, *blue bar*) is largely without effect. However, as we have shown previously (11), when both liposome populations contain the C terminally truncated Atlastin (1–471), fusion is largely abrogated in standard PC:PS liposomes (Fig. 7, *black bar*). Fusion is marginally improved with 10 mol% PE to roughly 9% of the wild type, whereas 20 mol% PE significantly improved *in vitro* fusion to roughly 31% of the wild type. In this reaction, neither fusion partner contains the C-terminal tail, yet fusion can occur at a reduced level. We also examined heterotypic fusion reactions that contained one C-terminal tail. The right half of Fig. 7*A* shows these results. A heterotypic interaction with one C-terminal tail in the PC:PS mixture was improved, and fusion approached wild-type levels when PE was included in the lipid mixture. As noted previously, the extent of fusion in the heterotypic reaction is dependent on the location of the mutant protein, in this case the C-terminal

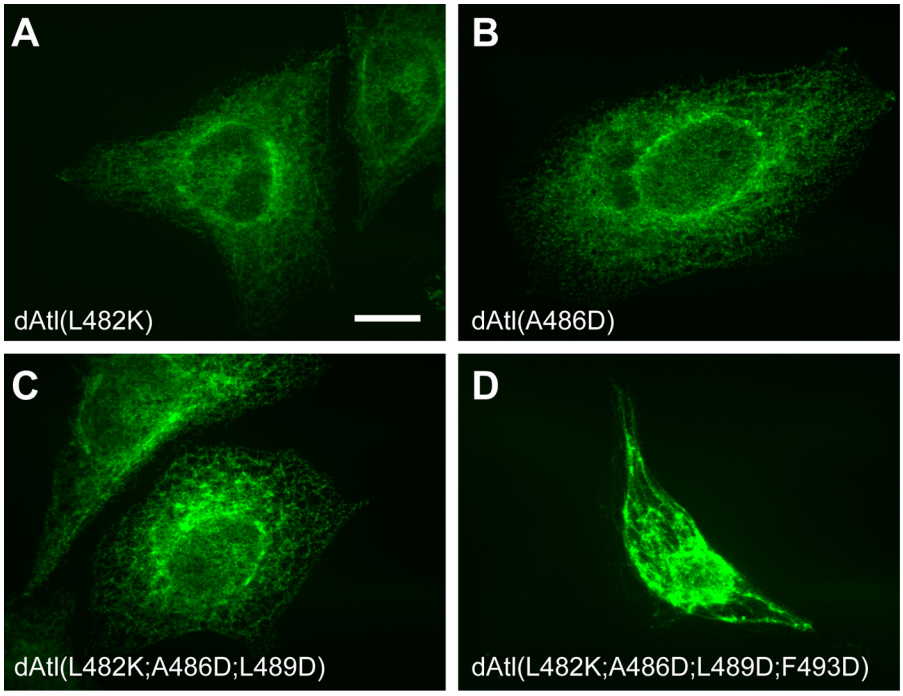

FIGURE 5. **Charge mutations in the C-terminal tail are more permissive *in vivo*.** Shown is a knockdown replacement assay. 48 h after transfection with the indicated Venus-dAtl constructs, cells were transfected with siRNAs targeting ATL2 and ATL3. 72 h after knockdown, Venus fluorescence was viewed by confocal microscopy. *A*, *Drosophila* Atlastin with a charge mutation in the amphipathic C-terminal tail, Venus-dAtl(L482K), is functional *in vivo* and can rescue the abnormal ER phenotype in cells treated with siRNA targeting Atl-2 and Atl-3. *B*, dAtl with a different charge mutation in the C-terminal tail, Venus-dAtl(A486D), is also functional *in vivo*. *C*, dAtl with three charge mutations in the C-terminal tail, Venus-dAtl(L482K;A486D;L489D), is functional *in vivo*. *D*, dAtl with four charge mutations in the C-terminal tail, Venus-dAtl(L482K;A486D;L489D;F493D), does not rescue the ER morphology. *Scale bar* = 10 μm.

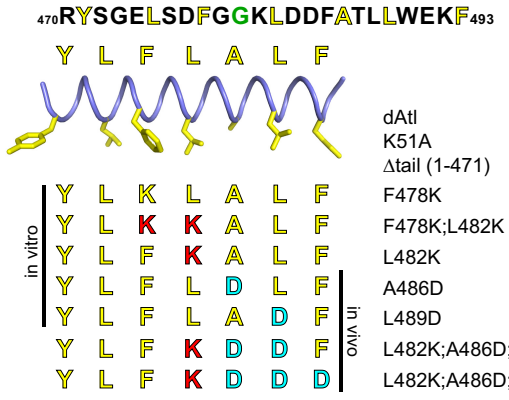

	in vitro fusion % of Wt	in vivo rescue % of Atl efficiency
dAtl	100	98.1
K51A	5	~0
Δtail (1-471)	5 (<5*)	20
F478K	66	nd‡
F478K;L482K	16	nd
L482K	21	98
A486D	<5*	97
L489D	<5*	nd
L482K;A486D;L489D	nd	79
L482K;A486D;L489D;F493D	~0	~0
G480K	104	nd

* Ref 12
‡ not determined

FIGURE 6. **Summary of *in vitro* and *in vivo* activity of *Drosophila* Atlastin C-terminal tail mutants.** *Left panel*, schematic of the C-terminal amphipathic helix with the amino acids forming the hydrophobic face highlighted in *yellow*. Seven mutations in the hydrophobic face of the C-terminal tail are shown below the schematic. Amino acids highlighted in *red* add a positive charge, and those highlighted in *blue* add a negative charge. The top five mutants were tested *in vitro*, whereas the bottom four were tested *in vivo*. *Right panel*, summary of the *in vitro* fusion activity of these mutants and their ability to rescue ER morphology in HeLa cells. The efficiency of plasmid recovery was determined as described previously (19). Briefly, Atlastin knockdown cells were transfected with various recovery plasmids, and the extent of the branched ER was determined by confocal microscopy. The fraction of cells that exhibited a branched ER morphology with *Drosophila* atlastin and atlastin mutants was determined and compared with recovery with human atlastin.

deletion, relative to the fluorescent lipid (Fig. 3*E*). Reconstitution efficiency is not affected by the addition of PE (Fig. 7*B*). The fusion activity of the L482K mutant was also improved by the addition of PE (Fig. 7*C*).

DISCUSSION

Membrane fusion requires phospholipids and other membrane components to undergo transitions that are energetically unfavorable and contrary to normal bilayer structure. Resident membrane proteins are responsible for encouraging these transitions and, ultimately, driving membrane merger. Membrane fusion driven by the GTPase Atlastin requires energy in the form of GTP hydrolysis as well as a conserved C-terminal amphipathic tail. Here we examine the role of this surface-active peptide during the process of membrane fusion. We found that a peptide corresponding to residues 470 and 492 of the

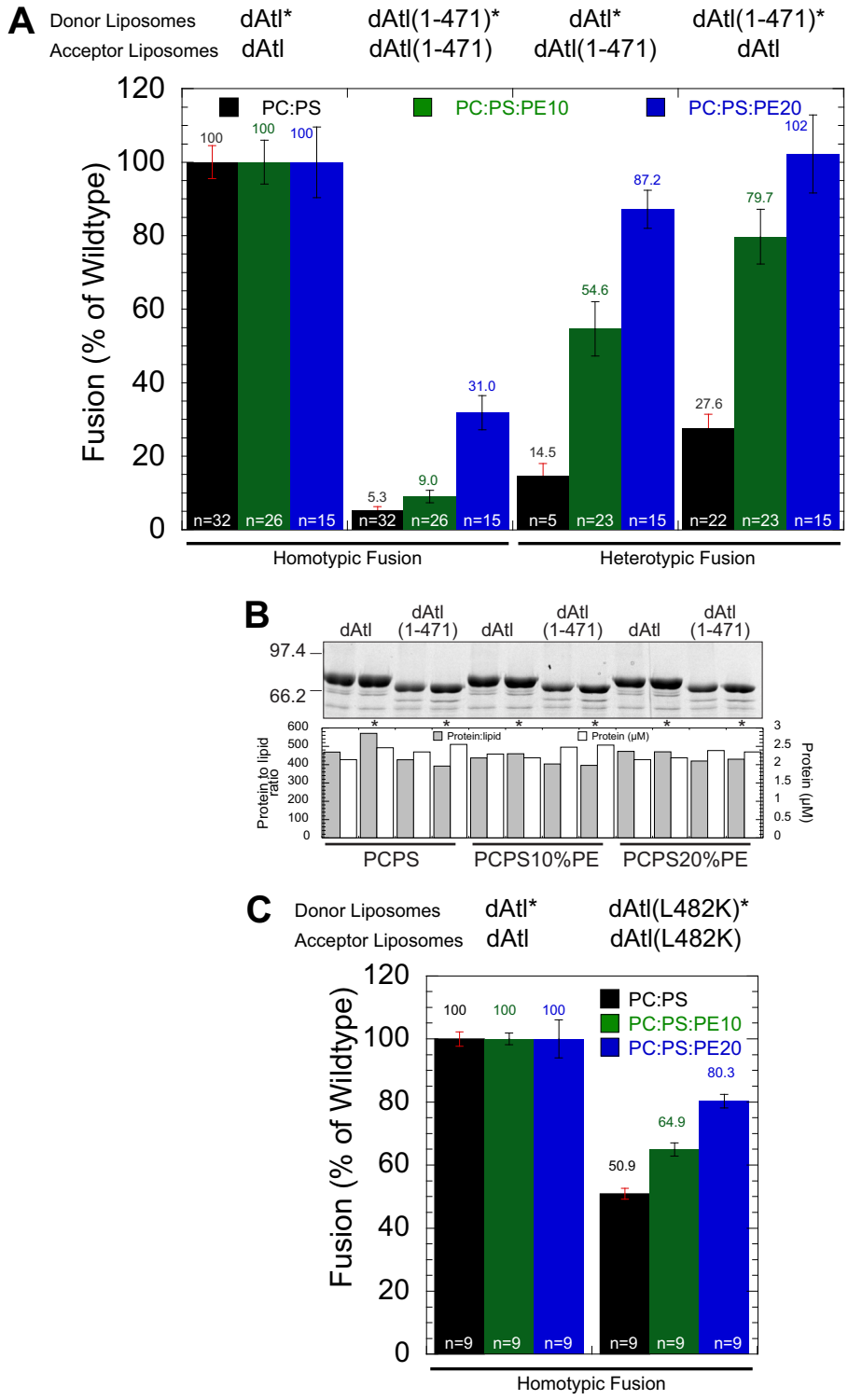

FIGURE 7. **Lipid composition strongly affects the requirements for the C-terminal amphipathic helix.** The extent of fusion at 60 min is represented in a histogram as the percentage of the wild type. *A*, the *left half* of the graph shows homotypic fusion reactions where the same protein is present in donor and acceptor liposomes. The *right half* shows heterotypic fusion reactions where mutant dAtl is present in one pool of liposomes, and wild-type dAtl is present in the other pool. Absolute levels of fusion (represented as a percentage of maximum fluorescence) ranged from 8.2–8.9% following background subtraction of ~0.9% found in the absence of GTP. The level of background fusion in the absence of GTP did not significantly differ with increased levels of PE. *Black*, PC:PS (85:15 mol%); green, PC:PS:PE (75:15:10 mol%); *blue*, PC:PS:PE (65:15:20 mol%). *Error bars* shown mean ± S.E. with the number of replicates (*n*) indicated in the histogram. *B*, Coomassie-stained SDS-PAGE gel of proteoliposomes. Protein:lipid ratios and protein concentrations were largely unaffected by addition of PE to the lipid mixes. Protein:lipid ratios ranged from 1:453 to 1:583 (protein concentrations of 2.2–1.63 μM) in PCPS; from 1:426 to 1:566 (2.34–1.77 μM) in PCPS, 10% PE; and from 1:392 to 1:600 (2.54–1.42 μM) in PCPS, 20% PE. Similar reconstitution efficiencies were seen with the 1–471 mutant in various lipid mixes. *C*, the fusion activity of the L482K mutant is similarly improved by increasing PE.

Drosophila Atlastin interacts with membranes and does so in a manner consistent with bilayer perturbation (Fig. 1). A recent study (20) found that a similar peptide (residues 479–507) also binds to membranes and can serve its required role when added in *trans* as a soluble peptide in an *in vitro* fusion reaction.

The amphipathic nature of the C-terminal tail is conserved across species, and membrane-perturbing activity is also transplantable from human Atlastin-1 and Atlastin-3 to *Drosophila* Atlastin (Fig. 2). A continuous hydrophobic face is required for normal Atlastin function because replacement of conserved hydrophobic side chains with charged residues reduces the ability of Atlastin to drive fusion *in vitro* (Fig. 3). However, this requirement is less stringent *in vivo* (Fig. 5). We found that *Drosophila* Atlastin can functionally replace human Atlastin-2 and Atlastin-3 in HeLa cells and restore ER morphology. However, a GTP binding mutant, K51A, does not rescue (Fig. 4*C*), nor does a truncated Atlastin lacking the conserved amphipathic tail (Fig. 4*D*). The hydrophobic character of the amphipathic helix is also important *in vivo*, but much more significant perturbation is required to influence the ability of dAtl to rescue Atl-2/3 knockdown (Figs. 5 and 6). One likely reason for the decreased sensitivity to Atlastin tail mutation *in vivo* is the effect of membrane composition. Our *in vitro* studies utilized a very simple lipid composition, in most cases a single phospholipid. The endogenous lipid composition of the ER membrane (27) is much more complex and will influence membrane curvature and surface interactions, among others. To test this possibility more directly, we altered the lipid composition of our *in vitro* fusion reaction to include increasing concentrations of the non-bilayer-forming lipid PE. The net effect of PE inclusion is to destabilize the membrane by providing an increased ability to undergo curvature transition. With increasingly destabilized bilayers, we found a decreased requirement for the C-terminal tail (Fig. 7*A*). In essence, the destabilizing function of the C-terminal tail is unnecessary when the bilayer is composed of an inherently unstable mixture.

The mechanical nature of the amphipathic C-terminal tail is also supported by the results of heterotypic fusion experiments. The graded fusion response with one functional C-terminal tail with increasing PE (Fig. 7*A*, *right*) shows that bilayer perturbation is not required for both fusion partners. This is also true of the point mutation L482K in pure PC bilayers because a point mutant on either side of the fusion reaction yields an intermediate fusion response (Fig. 3*B*). These observations show that mutations with the C-terminal tail are biochemically recessive, which is fundamentally different from mutations within the GTPase domain, such as K51A or R48A, which are biochemically dominant (6, 11), consistent with the genetic dominance of homologous mutations in animals.

Membrane fusion driven by Atlastin appears to combine mechanistic features of both SNARE-mediated fusion and type I virus-mediated fusion. Sequences within the transmembrane domain(s) are important (20), as are regions that perturb the bilayer structure (Fig. 1), such as viral fusion peptides (28). The GTPase requirement that likely drives conformational changes (29–31) necessary for fusion may be analogous to Rab proteins that influence the assembly of SNARE proteins (32). Future analysis of the Atlastin fusion mechanism will most likely reveal new features of this unique process.

REFERENCES

1. Wickner, W., and Schekman, R. (2008) Membrane fusion. *Nat. Struct. Mol. Biol.* **15,** 658–664
2. McNew, J. A. (2008) Regulation of SNARE-mediated membrane fusion during exocytosis. *Chem. Rev.* **108,** 1669–1686
3. McNew, J. A., Sondermann, H., Lee, T., Stern, M., and Brandizzi, F. (2013) GTP-dependent membrane fusion. *Annu. Rev. Cell Dev. Biol.* **29,** 529–550
4. English, A. R., and Voeltz, G. K. (2013) Endoplasmic reticulum structure and interconnections with other organelles. *Cold Spring Harb. Perspect. Biol.* **5,** a013227
5. Goyal, U., and Blackstone, C. (2013) Untangling the web: mechanisms underlying ER network formation. *Biochim. Biophys. Acta* **1833,** 2492–2498
6. Orso, G., Pendin, D., Liu, S., Tosetto, J., Moss, T. J., Faust, J. E., Micaroni, M., Egorova, A., Martinuzzi, A., McNew, J. A., and Daga, A. (2009) Homotypic fusion of ER membranes requires the dynamin-like GTPase Atlastin. *Nature* **460,** 978–983
7. Hu, J., Shibata, Y., Zhu, P. P., Voss, C., Rismanchi, N., Prinz, W. A., Rapoport, T. A., and Blackstone, C. (2009) A class of dynamin-like GTPases involved in the generation of the tubular ER network. *Cell* **138,** 549–561
8. Evans, K., Keller, C., Pavur, K., Glasgow, K., Conn, B., and Lauring, B. (2006) Interaction of two hereditary spastic paraplegia gene products, spastin and atlastin, suggests a common pathway for axonal maintenance. *Proc. Natl. Acad. Sci. U.S.A.* **103,** 10666–10671
9. Park, S. H., Zhu, P. P., Parker, R. L., and Blackstone, C. (2010) Hereditary spastic paraplegia proteins REEP1, spastin, and atlastin-1 coordinate microtubule interactions with the tubular ER network. *J. Clin. Invest.* **120,** 1097–1110
10. Chen, S., Novick, P., and Ferro-Novick, S. (2012) ER network formation requires a balance of the dynamin-like GTPase Sey1p and the Lunapark family member Lnp1p. *Nat. Cell Biol.* **14,** 707–716
11. Moss, T. J., Andreazza, C., Verma, A., Daga, A., and McNew, J. A. (2011) Membrane fusion by the GTPase atlastin requires a conserved C-terminal cytoplasmic tail and dimerization through the middle domain. *Proc. Natl. Acad. Sci. U.S.A.* **108,** 11133–11138
12. Liu, T. Y., Bian, X., Sun, S., Hu, X., Klemm, R. W., Prinz, W. A., Rapoport, T. A., and Hu, J. (2012) Lipid interaction of the C terminus and association of the transmembrane segments facilitate atlastin-mediated homotypic endoplasmic reticulum fusion. *Proc. Natl. Acad. Sci. U.S.A.* **109,** E2146–E2154
13. Hoff, K. G., Culler, S. J., Nguyen, P. Q., McGuire, R. M., Silberg, J. J., and Smolke, C. D. (2009) *In vivo* fluorescent detection of Fe-S clusters coordinated by human GRX2. *Chem. Biol.* **16,** 1299–1308
14. Sun, T. L., Sun, Y., Lee, C. C., and Huang, H. W. (2013) Membrane permeability of hydrocarbon-cross-linked peptides. *Biophys. J.* **104,** 1923–1932
15. Wu, Y., Huang, H. W., and Olah, G. A. (1990) Method of oriented circular dichroism. *Biophys. J.* **57,** 797–806
16. Schaffner, W., and Weissmann, C. (1973) A rapid, sensitive, and specific method for the determination of protein in dilute solution. *Anal. Biochem.* **56,** 502–514
17. Rigaud, J. L., and Lévy, D. (2003) Reconstitution of membrane proteins into liposomes. *Methods Enzymol.* **372,** 65–86
18. Rigaud, J. L., Pitard, B., and Levy, D. (1995) Reconstitution of membrane proteins into liposomes: application to energy-transducing membrane proteins. *Biochim. Biophys. Acta* **1231,** 223–246
19. Morin-Leisk, J., Saini, S. G., Meng, X., Makhov, A. M., Zhang, P., and Lee, T. H. (2011) An intramolecular salt bridge drives the soluble domain of GTP-bound atlastin into the postfusion conformation. *J. Cell Biol.* **195,** 605–615
20. Graf, E. R., Valakh, V., Wright, C. M., Wu, C., Liu, Z., Zhang, Y. Q., and DiAntonio, A. (2012) RIM promotes calcium channel accumulation at active zones of the *Drosophila* neuromuscular junction. *J. Neurosci.* **32,** 16586–16596

21. Wu, Y., He, K., Ludtke, S. J., and Huang, H. W. (1995) X-ray diffraction study of lipid bilayer membranes interacting with amphiphilic helical peptides: diphytanoyl phosphatidylcholine with alamethicin at low concentrations. *Biophys. J.* **68,** 2361–2369
22. Podbilewicz, B. (2014) Virus and cell fusion mechanisms. *Annu. Rev. Cell Dev. Biol.* **30,** 111–139
23. Jackson, M. B., and Chapman, E. R. (2006) Fusion pores and fusion machines in Ca^{2+}-triggered exocytosis. *Annu. Rev. Biophys. Biomol. Struct.* **35,** 135–160
24. Hoppins, S., and Nunnari, J. (2009) The molecular mechanism of mitochondrial fusion. *Biochim. Biophys. Acta* **1793,** 20–26
25. Pendin, D., Tosetto, J., Moss, T. J., Andreazza, C., Moro, S., McNew, J. A., and Daga, A. (2011) GTP-dependent packing of a three-helix bundle is required for Atlastin-mediated fusion. *Proc. Natl. Acad. Sci. U.S.A.* **108,** 16283–16288
26. Cohen, F. S., and Melikyan, G. B. (2004) The energetics of membrane fusion from binding, through hemifusion, pore formation, and pore enlargement. *J. Membr. Biol.* **199,** 1–14
27. Brügger, B. (2014) Lipidomics: analysis of the lipid composition of cells and subcellular organelles by electrospray ionization mass spectrometry. *Annu. Rev. Biochem.* **83,** 79–98
28. Skehel, J. J., Cross, K., Steinhauer, D., and Wiley, D. C. (2001) Influenza fusion peptides. *Biochem. Soc. Trans.* **29,** 623–626
29. Bian, X., Klemm, R. W., Liu, T. Y., Zhang, M., Sun, S., Sui, X., Liu, X., Rapoport, T. A., and Hu, J. (2011) Structures of the Atlastin GTPase provide insight into homotypic fusion of endoplasmic reticulum membranes. *Proc. Natl. Acad. Sci. U.S.A.* **108,** 3976–3981
30. Byrnes, L. J., and Sondermann, H. (2011) Structural basis for the nucleotide-dependent dimerization of the large G protein atlastin-1/SPG3A. *Proc. Natl. Acad. Sci. U.S.A.* **108,** 2216–2221
31. Byrnes, L. J., Singh, A., Szeto, K., Benvin, N. M., O'Donnell, J. P., Zipfel, W. R., and Sondermann, H. (2013) Structural basis for conformational switching and GTP loading of the large G protein atlastin. *EMBO J.* **32,** 369–384
32. Barr, F. A. (2013) Review series: Rab GTPases and membrane identity: causal or inconsequential? *J. Cell Biol.* **202,** 191–199